

Kondo induced π -phase shift of microwave photons in a circuit quantum electrodynamics architecture

Guang-Wei Deng ^{1,2,*}, Loïc Henriët,^{3,*} Da Wei,^{1,2} Shu-Xiao Li,^{1,2} Hai-Ou Li,^{1,2} Gang Cao,^{1,2} Ming Xiao,^{1,2} Guang-Can Guo,^{1,2} Marco Schiró,⁴ Karyn Le Hur,³ and Guo-Ping Guo ^{1,2,†}

¹Key Laboratory of Quantum Information, University of Science and Technology of China, Chinese Academy of Sciences, Hefei, Anhui 230026, China

²Synergetic Innovation Center of Quantum Information & Quantum Physics, University of Science and Technology of China, Hefei, Anhui 230026, China

³Centre de Physique Théorique, École polytechnique, CNRS, Université Paris-Saclay, F-91128 Palaiseau, France

⁴Institut de Physique Théorique, Université Paris Saclay, CNRS, CEA, F-91191 Gif-sur-Yvette, France



(Received 14 September 2020; revised 24 June 2021; accepted 16 August 2021; published 3 September 2021)

The Kondo effect refers to the screening of a spin-1/2 impurity by a cloud of conduction electrons, then forming a many-body Fermi liquid ground state. Theoretical calculations suggest that the Kondo resonance can interact with light and should give rise to a π -phase shift of the photon signal in the case where the ground state is a Fermi liquid. This π -phase shift of light is driven from the Korrington-Shiba relation of quantum impurity Fermi-liquid ground states. We report the first observation of such a π -phase shift in a graphene double quantum dot within a circuit quantum electrodynamics architecture where the microwave photons couple to the pseudospin or charge degrees of freedom. We study the evolution of the π -phase shift as a function of temperature and bias voltage. The observed Kondo temperature $T_K \sim 550$ mK is in agreement with dc conductance measurements. All our results support the formation of a Kondo resonance located above the Fermi level of the electronic reservoirs with the occurrence of an $SU(4)$ Fermi-liquid ground state. We finally study how the Kondo-photon interaction can be tuned by inter-dot electron tunnel coupling strengths. Our findings may contribute to a better understanding of many-body physics in hybrid circuit systems, and open up applications in atomic thin materials from the light-matter interaction.

DOI: [10.1103/PhysRevB.104.125407](https://doi.org/10.1103/PhysRevB.104.125407)

I. INTRODUCTION

A lot of efforts have been carried out to study Kondo physics in quantum dot and mesoscopic geometries [1–8]. The occurrence of a Kondo resonance at the mesoscale produces a phase shift in the transmitted electronic wave packet, which depends on the symmetry and nature of the many-body ground state [9–12]. Recently, advances in circuit quantum electrodynamics (cQED) architectures have been used to detect charge or orbital degrees of freedom and reveal the effect of charge fluctuations in the Kondo effect [13–20], which offer an appealing platform to study many-body physics and light-matter interactions. Previous theory predicted that the Kondo effect could be suppressed by irradiation [21]. Photon-induced Kondo satellites in a single-electron transistor [22], microwave-induced charge frozen at Kondo resonance [16], and scaling laws of the Kondo problem at finite frequency [20] have been reported. However, the backaction effect of the Kondo correlation on the irradiation field, such as the coupled microwave field, has not been yet demonstrated. In particular, a Kondo effect is predicted to give rise to a π -phase shift of the microwave photon signal at resonance in the case where the

ground state is a Fermi liquid [23,24]. In this paper, we report the observation of such a π -phase shift of light in a double quantum dot (DQD) system, where the two dots are strongly capacitively coupled, and we study the associated many-body physics.

Such a double quantum dot system has been predicted to reveal $SU(4)$ Kondo correlations with entangled spin and charge degrees of freedom [25–28]. The occurrence of the π -phase shift of light can in fact be understood from general arguments related to quantum impurity physics. In the Kondo model, the spin or here the pseudospin related to the charge or orbital degrees of freedom on the two dots, is described by a dynamical susceptibility $\chi(\omega)$, which describes the response to an applied ac field. If one fixes the frequency of the ac field to be close to the resonance frequency of the many-body system ω_K such that $\hbar\omega_K = k_B T_K$, with \hbar and k_B being the Planck and the Boltzmann constants, then one obtains the important equality $J(\omega_K)\chi(\omega_K) = -i$ [according to Eq. (1.1) below] [23,24] showing the Fermi liquid ground state formation [27–29]. Here, $J(\omega)$ represents the spectral function associated to the transmission channel, which transports the microwave signal. This relation that holds for $\omega = \omega_K$ implies a form of dynamical spin susceptibility in agreement with the Korrington-Shiba relation of quantum impurity Fermi liquid systems at low frequencies [30,31]. This relation leads to important predictions for many-body Kondo physics and

*These authors contributed equally to this work.

†Corresponding author: gpguo@ustc.edu.cn

charge fluctuations in quantum RC circuits at low frequencies [32–36]. Here, we generalize the analysis to the regime $\omega \sim \omega_K$ by coupling to the microwave channel or a transmission line. If we couple directly the pseudospin to the transmission line, the reflection coefficient of the microwave photon

$$S_{11}(\omega) = Ae^{i\phi} = 1 - 2iJ(\omega)\chi(\omega) \quad (1.1)$$

shows a $\Delta\phi = \pi$ -phase shift for the resonance condition $\omega = \omega_K$ [23,24,37]. This π -phase shift of microwave photons should occur when fixing the photon frequency ω in resonance with the many-body frequency ω_K , assuming the ground state is a quantum-impurity Fermi liquid system.

It is relevant to emphasize that for an open transmission line, $\Delta\phi = 0$ [38]. This shows that many-body physics is important in the present case and directly measurable from the photon phase shift. This phase of the reflected light signal is also different from the Friedel's phases $\delta = \pi/2$ and $\pi/4$, which have been observed in the dc electronic conductance $(2e^2/h)\sin^2\delta$ for the $SU(2)$ [1–3,12] and $SU(4)$ Kondo effects [4–7,39], respectively.

Below, we precisely reveal the π -phase shift of the photon signal by coupling a graphene DQD with a microwave resonator. Our study of the microwave photon response supported by dc conductance measurements across the mesoscopic electron system agrees with an $SU(4)$ Kondo model, which shows entangled spin and charge degrees of freedom [25–28], and with a Kondo resonance located above the Fermi energy evolving with temperature and bias voltage. In Ref. [40], low-frequency measurements of microwave light in carbon nanotube systems were performed in accordance with theory, and the authors reported a phase in radians, which was not too small, still measured away from resonance such that the π -phase value was not attained. It is also relevant to mention here that a Kondo effect was measured in graphene with point defects (vacancies) [41] and was not reported before in graphene quantum-dot systems [42,43]. Our paper then shows the possibility of Kondo physics in graphene quantum dots. Another very recent work has also revealed Kondo physics in graphene quantum dots [44]. To show the robustness of the results, we present two cooling procedures and analyze different samples. We will also study the effect of tuning (increasing) the tunneling strength between the two dots.

To analyze the data, we build a microscopic model describing the coupling of the mesoscopic DQD system with the circuit quantum electrodynamics (cQED) architecture. This will then give rise to a quantized mode model or an harmonic oscillator with a bare frequency ω_0 transporting the microwave power. The capacitive light-matter coupling will result in a many-body shift of this frequency ω_0 , leading to a resonant condition called ω_0^* and englobing the formation of the Kondo resonance related to T_K . We will build a theory to show how the light precisely develops a π -phase shift at the frequency ω_0^* corresponding to this specific geometry. Regarding the description of the electronic reservoirs, we consider that the DQD size is much larger than the atomic distance between neighboring sites in graphene, such that only the symmetric wave function associated to sublattices A and B points of the honeycomb lattice couple to the mesoscopic system [Fig. 1(d)]. This leads to a one-channel description in each electronic reservoir in addition to the spin flavor, as in

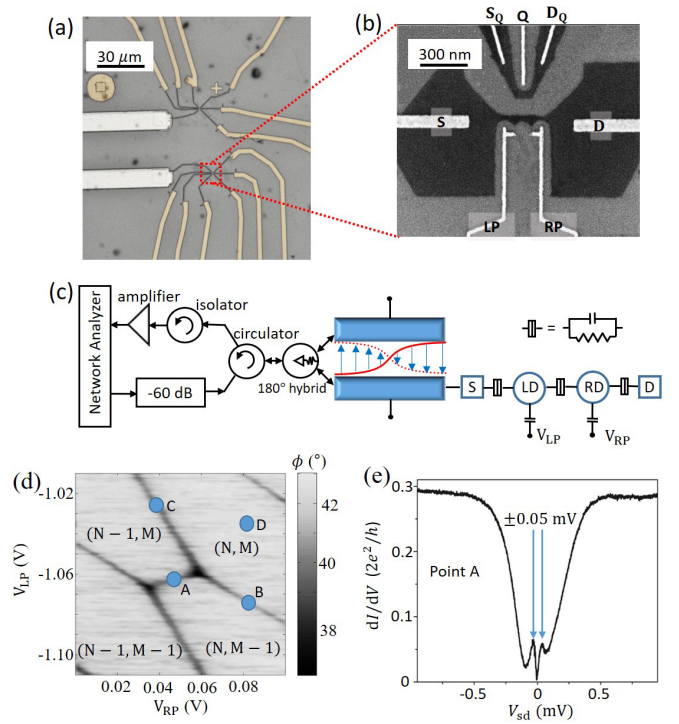


FIG. 1. Sample structure of the graphene DQD and transport peaks at small bias voltages. (a) Micrograph of the DQD gate structure. (b) Sample structure of a typical etched graphene DQD. The dc voltages used to control the charge numbers in the DQD are applied via left and right plunger (LP and RP) gates. A quantum point contact with a source (SQ) and drain (DQ) channel and a tuning gate (Q) is integrated near the DQD. (c) Schematics of the hybrid device. The half-wavelength reflection line resonator is connected to DQD's left dot (LD) at one end of its two stripelines. The right dot (RD) is connected to the drain. A microwave signal is applied to the other end of the resonator, and the reflected signal is detected using a network analyzer. (d) Charge stability diagram of the DQD measured by dispersive readout with the resonator. The gate lever arms are 10% in Fig. 9. (e) Differential conductance at point A from panel (d), showing two peaks at finite voltage $V_{sd} \sim \pm 0.05$ mV.

the $SU(4)$ Kondo effect [25]. We assume that the chemical potential does not lie at the neutrality point, to have a finite density of states in the reservoirs, enabling us to observe the Kondo effect [45].

The organization of the article is as follows. In Sec. II, we introduce the device, its characterization and show the appearance of the $SU(4)$ Kondo effect at the charge degeneracy points of the DQD from the formation of a two-peak structure in electron transport across the mesoscopic system at low temperature. We carefully analyze the data to deduce microscopic parameters. Then, in Sec. III, we demonstrate the quantization of the light phase shift to the π value and analyze the light-matter coupling properties. In particular, we also show that such a π -phase shift progressively attenuates above the Kondo temperature. To be sure of our findings, we show results on different samples. In Sec. IV, we show how the data can be fitted through a Kondo model with $SU(4)$ symmetry. Although the π -phase shift of light is a property of Fermi liquid ground states and therefore can also occur for $SU(2)$

Kondo effects, here we show that the results are in agreement with a Kondo resonance peaked above the Fermi energy. The theory also shows from renormalization group arguments on interaction effects in the Kondo resonance why the π shift of light is in fact robust up to energy scales larger than the Kondo energy scale, i.e., here ~ 10 times the Kondo energy scale referring then to energies of the order of the charging energy. This fact also justifies that the π -phase shift of light could not be explained through a noninteracting resonant level model to describe the dynamics of the DQD. In Sec. V, we study the effect of increasing the microwave power in the Coulomb blockade regime and show that it can restore the π -phase shift of light, in accordance with theoretical predictions. In Sec. VI, we summarize our results and address final remarks. Appendices are devoted to additional information on the sample characteristics, light-matter analysis, and theoretical Kondo analysis.

II. SAMPLE CHARACTERIZATION AND OBSERVATION OF KONDO EFFECT

The device shown in Figs. 1(a) and 1(b) is mounted in a dilution refrigerator, its base temperature is about 30 mK.

Our previous works on graphene double quantum dots were performed both in series [46] and in parallel [47] shapes, allowing us to tune with precision the double dot orbital levels with dc gates. Two DQDs, made of few-layer etched graphene, are coupled to the resonator through their sources [48], however, only one of them is used while the other is grounded throughout the course of present experiment. Transport measurements are performed through source and drain [Fig. 1(b)], and the charge stability diagram is achieved by adjusting the gate voltages V_{LP} and V_{RP} [Fig. 1(d)]. The electronic temperature of the DQD at base temperature is estimated to be about 100 mK, which has been reported by a temperature dependence experiment [49]. A vector network analyzer (VNA) is used to apply coherent microwave driving tone and measure the reflection signal S_{11} [defined from the scattering matrix, see Fig. 1(c)]. The reflection signal can be measured by its amplitude ($A = |S_{11}|$) and phase [$\phi = \arg(S_{11})$] components through the VNA. The resonance frequency of the resonator is 6.35 GHz, with a quality factor of ~ 3000 . Details of sample fabrication and measurement setup are shown in Appendix A.

A dispersive readout measurement permits to obtain the charge stability diagram of the DQD system [see Fig. 1(d)] [49], which shows the equilibrium charge state of the two dots as a function of the gate voltages V_{LP} and V_{RP} . This diagram shows a typical hexagonal structure [2]. At point D, the electronic configuration (N, M) corresponds to N electrons in the left dot and M electrons in the right dot. Along the grey lines (points A, B, and C), two charge configurations are degenerate. By maintaining the electrochemical potential of one dot, we establish the Coulomb diamond of the other dot in Fig. 9 of Appendix A. From this method, we find the charging energy of both dots to be $E_C \sim 0.4$ meV, and from the charge stability diagram the mutual capacitance between dots is comparable to the single-dot capacitances [48]. Note that the gate lever arms are 10% in Fig. 9.

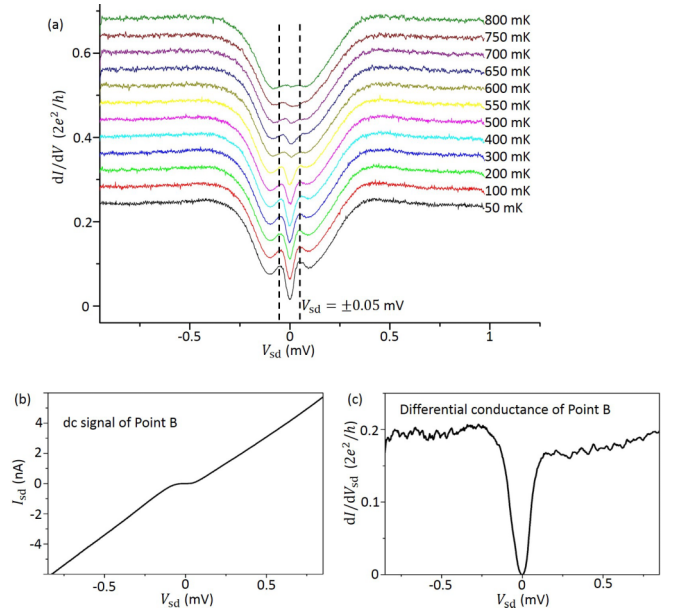


FIG. 2. (a) Temperature profile of the dI/dV conductance in units of $2e^2/h$ at the point A showing the formation of a two-peak structure at an energy scale comparable to the the Kondo temperature $T_K = 550$ mK. The low-temperature properties are in agreement with the formation of an $SU(4)$ Kondo effect [25,28]. [(b),(c)] For a comparison, we show transport properties at point B for the temperature $T = 30$ mK.

Below, we study in more detail the charge degeneracy point A, where the pseudospin will correspond to the two degenerate charge states $(N - 1, M)$ and $(N, M - 1)$, with one state on each quantum dot.

First, we show the occurrence of Kondo physics in electron transport across the mesoscopic system. We measure the differential conductance dI/dV at point A (as a function of source-drain voltage or bias voltage V_{sd}), which reveals two peaks at $V_{sd} \sim \pm 0.05$ mV [Figs. 1(e) and 2(a)]. From the Fermi-liquid approach to the $SU(4)$ Kondo effect, in the limit of small bias voltages $V_{sd} \rightarrow 0$ across the DQD with $e|V_{sd}| = \hbar\omega$, the conductance essentially takes the form $(2e^2/h)k_B T_K \rho(\hbar\omega = e|V_{sd}|)(|t'|/(k_B T_K))^2$ [25] where the factor $(|t'|/(k_B T_K))^2$ corresponds to the transmission probability through the DQD and the electron spectral function ρ englobes the formation of the Kondo resonance in the density of states. The electron spectral function $\rho(\omega)$ at zero-bias voltage and in the quantum limit reads

$$\rho(\omega) = \frac{1}{\pi} \frac{k_B T_K}{(\hbar\omega - \epsilon_0)^2 + (k_B T_K)^2}, \quad (2.1)$$

where ϵ_0 is the position of the Kondo resonance and T_K the Kondo temperature. A peculiarity of the $SU(4)$ Kondo effect is that the Kondo resonance is located above the Fermi energy at $\epsilon_0 \sim k_B T_K$ such that $\rho(0) \sim 1/(2\pi k_B T_K)$ in the limit of zero-frequency. The additional factor $1/2$ in the denominator of $\rho(0)$ for the $SU(4)$ Kondo effect is in agreement with a $\delta = \pi/4$ -phase shift, which then leads to $G(0) = G_0 \sin^2 \delta$ with $G_0 = (2e^2/h) \frac{1}{\pi} (|t'|/(k_B T_K))^2$ referring to the conductance value for an $SU(2)$ Kondo effect with a $\pi/2$ -phase shift. The data are in good agreement with the $SU(4)$ Kondo

effect. From the low-temperature limit in Fig. 2(a), we identify $G(0)h/(2e^2) \sim 0.015$ for $k_B T \sim 50$ mK such that this formula gives $t' \sim 0.3k_B T_K$ if we set $\epsilon_0 \sim k_B T_K$ such that $G(0) = (2e^2/h) \frac{1}{2\pi} (|t'|/(k_B T_K))^2$. This value of t' is justified from the microwave response [46]. To obtain the Kondo temperature T_K , we analyze the data at finite voltages.

The presence of anomalies at $V_{sd} \sim \pm 0.05$ mV also agrees with a spectral function ρ described by a resonance at $\epsilon_0 = eV_{sd} = k_B T_K$ above the Fermi energy of the reservoir electron leads, as predicted by the theory. These two peaks in the dI/dV electronic transport response occur for an electron energy $eV_{sd} \sim 50 \mu\text{eV}$, which corresponds to a Kondo temperature $T_K \sim 550$ mK. These two peaks traduce the position of the Kondo resonance above the Fermi energy. The $SU(2)$ Kondo effect would show a maximum at zero bias-voltage. We also verify the formation of the $SU(4)$ Kondo effect through the linear increase of the conductance at small voltages. We find that the correction in the conductance from the zero-bias value evolves as $\sim \frac{15\pi}{4} (eV_{sd}/k_B T_K)$ in units of G_0 . This correction comes from the evolution of the Friedel's phase shift $\delta = \frac{\pi}{4} + \frac{15}{4}\pi\lambda\omega$ with $\lambda = a/(k_B T_K)$ and a is a parameter of the order of unity in the quantum field theory description of the Fermi liquid (see Appendix B of Ref. [28] related to Ref. [50]) where we set $\omega = eV_{sd}$ in $G = G_0 \sin^2 \delta$. The order of magnitude of the correction predicted from the theory is in agreement with data, which shows that the linear dI/dV increases rapidly from 0 to $k_B T_K$ roughly from a factor 10^1 , resulting in $G(eV_{sd} \sim k_B T_K) \sim 0.1(2e^2/h)$. For a comparison, in Fig. 2(c), we show the conductance at point B in the phase diagram. The conductance is zero at $V_{sd} = 0$ and the signal does not show satellite peaks.

We also study the temperature effects in Fig. 2(a), showing that the two-peak structure precisely forms at the Kondo temperature scale. Here, we observe that the conductance at low-bias voltages remains almost identical for temperatures from 50 mK to 400 mK traducing a robustness towards temperature effects. This is also in agreement with the Fermi liquid theory applied to the $SU(4)$ Kondo effect, which predicts $(T/T_K)^3$ corrections for the conductance whereas the Kondo effect with $SU(2)$ symmetry would result in $(T/T_K)^2$ temperature corrections [28].

The dI/dV characteristics is therefore useful to detect the $SU(4)$ Kondo effect because it reflects the spectral function on the mesoscopic system, which is known for the $SU(4)$ Kondo effect to show peaks not at the Fermi level, but rather at the positions $\pm k_B T_K$ in bias voltages [28]. The mesoscopic system then behaves similarly as an interacting resonant level system centered at the position $\epsilon_0 = k_B T_K$, with a width Γ that will be studied below as a function of bias voltage and temperature and which could not be described in terms of a noninteracting resonant level model.

III. OBSERVATION OF π -PHASE SHIFT OF LIGHT

Here, we present the analysis for the light signal at the point A. Fixing gate voltages at point A, we measure the microwave photon response as a function of the source-drain voltage V_{sd} , in order to characterize the light-matter interaction.

In Figs. 3(a), 3(c), and 3(e), we present the results for the microwave signal, showing a phase shift of the order of π for

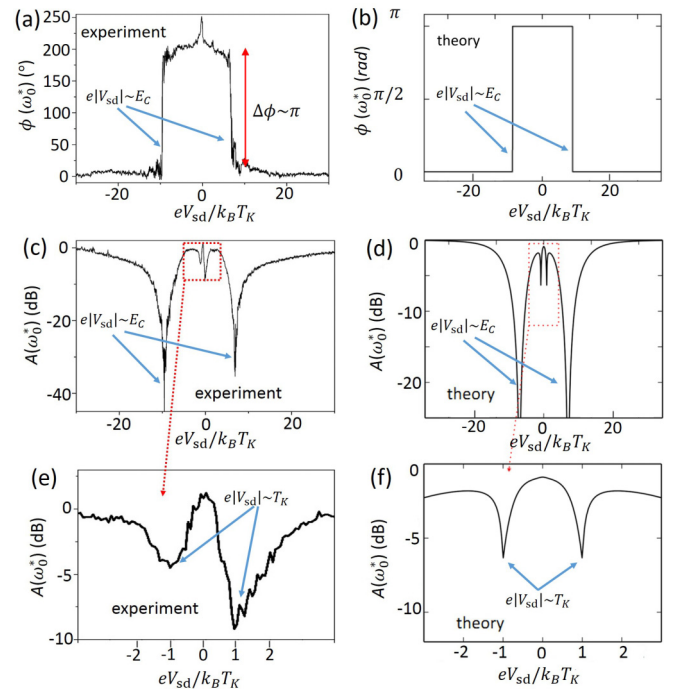


FIG. 3. Microwave measurements and theoretical results. (a) Experimental result for the phase $\phi(\omega_0^*)$ of the reflected signal $S_{11}(\omega_0^*)$ at point A and at resonance $\omega = \omega_0^*(V_{sd})$ and its evolution with respect to bias voltage. (b) Theory result for the phase based on the effective quantum impurity model. To fit the data, we obtain the light-matter coupling from the frequency shift in Fig. 10, and find $\lambda/(\hbar\omega_0^*) = 10^{-2}$; we test different values of the dissipation parameter α and find that results are quite robust to different values of α ; we choose $\alpha = 10^{-5}$. The Kondo energy scale $T_K \approx 550$ mK is obtained from a fit of the low-energy features. We find $t' \sim 0.3k_B T_K$ from the analysis of the dc conductance and from the microwave response. The parameter Γ is derived from the Fermi-liquid theory together with Eqs. (4.1). [(c),(e)] Experimental results for the amplitude A of the reflection coefficient $S_{11}(\omega_0^*)$ at point A, as a function of the bias voltage; the zoom focuses on low-energy features. [(d),(f)] Theory results based on the effective quantum impurity model.

a prominent window of bias voltages V_{sd} applied across the mesoscopic electron system. In addition, the amplitude of the signal also reveals two dips at low-energy scale, in agreement with that of Fig. 1(e). As shown in Fig. 3(a), a very robust phase of π is observed from $V_{sd} = 0$ to $V_{sd} \approx \pm 0.4$ mV, above which the phase suddenly drops to zero. In Fig. 3(c) the amplitude (in dB) shows also two pronounced dips around $V_{sd} \approx \pm 0.4$ mV. We notice that these features in the experimental results can be associated with an energy scale, which is comparable with the charging energy E_C .

For completeness, we also show the light responses at points B and C in the charge stability diagram. [See Fig. 4]. The light signals for the phase do not saturate to the quantized π value and the amplitude responses do not show the low-energy structure related to the Fermi-liquid ground state at the point A.

In the present geometry, the transmission line transporting the microwave power is described by the spectral function

$$J(\omega) = 2\alpha\omega e^{-\omega/\omega_c}, \quad (3.1)$$

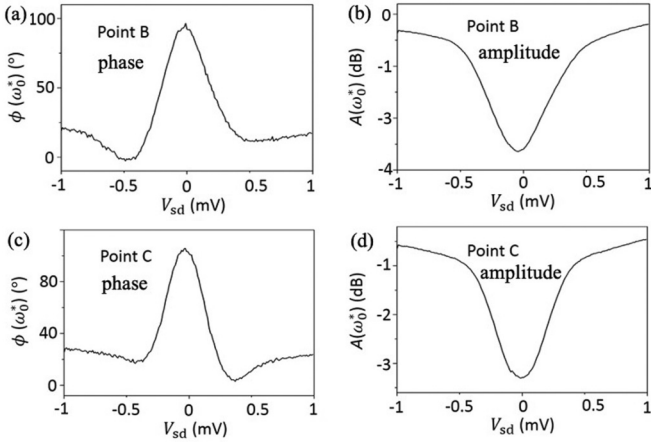


FIG. 4. Typical phase and amplitude responses at points B and C, as a function of bias voltage.

where the high-frequency cutoff ω_c is considered large compared to the driving frequency and the charging energy E_C . To fit the data, we assume that $\alpha \sim 10^{-5}$; this value of α can also account for other internal dissipation effects [51,52].

To evaluate the reflection coefficient S_{11} , we attach to the transmission line the cQED resonator (cavity), which is described by the photon field \hat{x} characterizing the quantization of the electric field inside the cavity. Here, we calibrate S_{11} in a form such that it agrees with a zero phase for the light signal at $\omega = \omega_0$ in the absence of any coupling with the mesoscopic electron system. From standard input-output theory [53], we obtain $S_{11}(\omega, V_{sd}) = -1 + 2iJ(\omega)\chi_{xx}^R(\omega, V_{sd})$, where the retarded dynamical susceptibility χ_{xx}^R associated with the microwave field can be tuned as a function of the bias voltage V_{sd} applied across the mesoscopic electron system and frequency of the microwave power. To agree with the definition of S_{11} here, we write the general form:

$$\chi_{xx}^R = \frac{\hbar\omega_0}{(\hbar\omega)^2 - (\hbar\omega_0)^2 - \hbar\omega_0\Pi^R(\omega) + iJ(\omega)\hbar\omega_0}, \quad (3.2)$$

which includes the contributions coming from coupling the cQED resonator with the electronic system through

$$\Pi^R = \text{Re}(\Pi^R) - i\text{Im}(\Pi^R), \quad (3.3)$$

and with the transmission line through $J(\omega)$. In particular, Π^R will traduce the formation of the Kondo resonance between the DQD and the electronic reservoirs. Through Eq. (3.2), the resonance condition for light is defined as

$$(\hbar\omega_0^*(V_{sd}))^2 = (\hbar\omega_0)^2 + \hbar\omega_0\text{Re}(\Pi^R(\omega_0^*(V_{sd}))). \quad (3.4)$$

We underline that the microwave results are obtained at the renormalized resonance frequency $\omega_0^*(V_{sd})$, which is determined from the minimum of the amplitude $A = |S_{11}|$ as a function of frequency (see Appendix B) [43].

Before describing in a quantitative manner the capacitive coupling between the resonator and the mesoscopic electron circuit, we can pursue at a general level the theoretical discussion on the occurrence of the π -phase shift. More precisely, from Eqs. (3.2) and (3.4), we deduce that $\chi_{xx}^R(\omega_0^*)(\text{Im}\Pi^R(\omega_0^*) + J(\omega_0^*)) = -i$, which is a generalization of the formula mentioned in the introduction for the spin

susceptibility. When $\Pi^R(\omega_0^*) = 0$ we check that $S_{11} = 1$ in agreement with an open transmission line. On the contrary, if dissipation effects on the cQED resonator comes from the coupling with the mesoscopic electron system forming the Kondo resonance, then the condition $\text{Im}\Pi^R(\omega_0^*) > J(\omega_0^*)$ will result in a π -phase shift in S_{11} .

This phase shift is not yet a (complete) proof of the formation of a many-body Kondo resonance because at this stage this just traduces that the cQED system couples more strongly with another medium than the transmission line, here the mesoscopic electron system, characterized by a resonance with a Lorentzian form for the electron spectral function. Then, in Fig. 5, we show the temperature evolution of the amplitude and phase of the microwave signal. Similarly as the dI/dV conductance, we verify that the π -phase shift of light is formed at the same Kondo temperature scale. The quantitative analysis developed in Sec. IV taking into account the renormalization effects in the width of this resonance, in agreement with the formation of a many-body Fermi liquid ground state, will justify the occurrence of such a π -phase shift of light until energies of the order of the charging energy. When increasing the bias voltage across the mesoscopic system, interaction-interaction effects in the Kondo resonance are well known to produce decoherence effects, which then increase considerably the width of the resonance with this bias voltage [54]. We will adapt this calculation of the resonance width and position to our system, showing that theory results of Figs. 3(b), 3(d), and 3(f) are in agreement with an $SU(4)$ Kondo effect.

In Fig. 6, we show results for a different device, referred to as device 2, with different tunnel coupling strengths t' for points A. Using similar methods as we discussed previously in device 1 (referring to the sample in the preceding section), we estimate the temperature scale T_K of device 2 to be ~ 600 mK (corresponding to an energy scale of ~ 12.2 GHz). For points 1 and 2 in Fig. 6(a), essentially $t' < k_B T_K$, therefore we obtain similar results as in Figs. 3 and 10 in Appendix B. In that case, t' does not enter in the low-energy description (see Appendix C). The phase shift observed in the microwave measurement in Fig. 6(d) progressively decreases from point 1 to point 3. For point 3, where $t' > k_B T_K$, the two dots are strongly coupled and form a molecule (large dot), which then enters in a strongly Coulomb blocked situation and almost decouple from the leads. The charge on the DQD becomes fixed to an integer value and the conductance through the DQD becomes zero in the limit of $V_{sd} \sim 0$. Equivalently, t' acts as an orbital magnetic field along X direction for the pseudospin (see Appendix C), which gradually suppresses the Kondo effect.

IV. THEORETICAL KONDO MODEL

To build the precise Kondo model and our quantitative analysis for the light-matter coupling, we introduce in addition to the spin $S_z = \pm 1/2$ of an electron, the orbital pseudospin quantum number $T_z = \pm 1$ associated with the two degenerate charge states on the DQD at point A. We first verify that the 4 quantum states on the DQD coupled to the symmetric wave function made of the sublattices (usually called A and B) in the graphene reservoir leads produce an

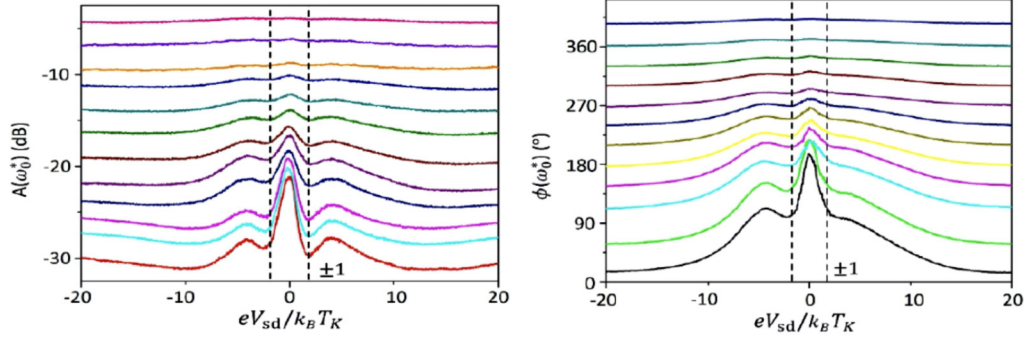


FIG. 5. Amplitude in decibels (dB) and phase in degree of the microwave signal for the same temperatures as in Fig. 2. We verify that the π -phase shift of light smoothly appears at the Kondo temperature scale $T_K \sim 550$ mK.

$SU(4)$ Kondo model. See Appendix C for further details on the theory.

Within this description of the electronic sector, the light-matter coupling, which describes the coupling between the resonator or cQED to the left lead in Fig. 1 can be written as a capacitive coupling to the orbital degree of freedom $\lambda T_z \hat{x}$, where λ quantifies the coupling between the cavity or the resonator and the mesoscopic electron system. Studying the evolution of ω_0^* with respect to the driving frequency in Appendix B, we deduce $\lambda/(\hbar\omega_0^*) = 10^{-2}$ and we adjust the value of ω_0^* for different voltages V_{sd} . To make a precise link with an interacting resonant level, it is useful to reformionize the pseudospin-1/2 particle: $T_z = 2(d^\dagger d - 1/2)$, $T^+ = d^\dagger$ and $T^- = d$, where the fermionic operators d and

d^\dagger describe the orbital degrees of freedom on the DQD. For a fixed value of the bias voltage V_{sd} , the associated spectral function ρ to this d -particle takes the precise form of Eq. (C2) in Appendix C. A diagrammatic analysis in Appendix C then leads to $\text{Im}\Pi^R(\omega_0^*) \sim \lambda^2 \text{Im}\chi(\omega_0^*)$, where $\chi(\omega)$ is the spin susceptibility introduced earlier. The Korringa-Shiba relation for $\chi(\omega)$ then gives the estimate $\text{Im}\Pi^R(\omega_0^*) \sim \lambda^2 (\hbar\omega_0^*)/T_K^2 \sim 10^{-4} \hbar\omega_0^*$, which then justifies that at low-bias voltages $\text{Im}\Pi^R(\omega_0^*) > J(\omega_0^*)$, resulting in the π -phase shift of light.

Within the same diagrammatic approach, we evaluate the bias-dependent resonant level width, and demonstrate in Appendix C that the formulas in Ref. [54]

$$\Gamma = k_B T_K \text{ for } eV_{sd} \ll k_B T_K$$

$$\Gamma \sim \frac{eV_{sd}}{\ln^2(eV_{sd}/k_B T_K)} \text{ for } eV_{sd} \gg k_B T_K, \quad (4.1)$$

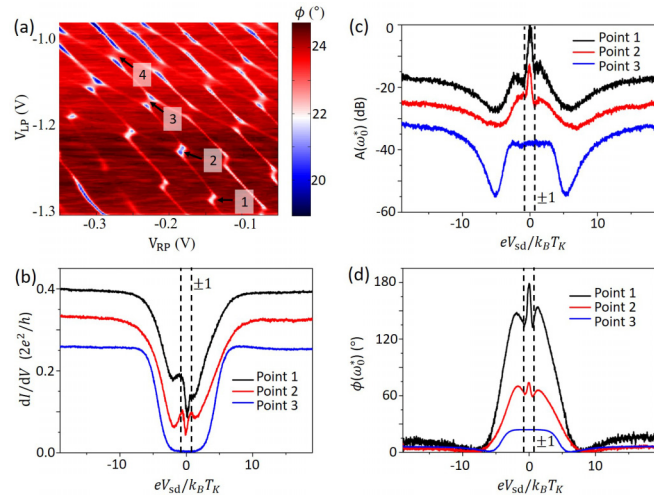


FIG. 6. Evolution of the results with inter-dot coupling strength t' for a second device. (a) Charge stability diagram for device 2. Inter-dot tunnel coupling strengths t' of point 1, 2, and 3 are fitted to be 5.8 GHz, 8.4 GHz, and 15.6 GHz, respectively, using a typical cavity response fitting procedure [15,49]. The point 4 shows a too large t' parameter to be characterized by our cavity measurements. (b) Electronic differential conductance across the DQD for points 1,2,3. (c) Amplitude and (d) phase response of the microwave light signal as a function of the bias voltage V_{sd} across the mesoscopic electron system for the three points 1, 2, 3. We observe that the phase shift of point 2 cannot reach 180 degree. Curves at points 1 and 2 in (b) have an offset of 0.5 and in (c) the offset is 10 dB.

are valid for an $SU(4)$ Kondo effect. See Eq. (C7) in Appendix C for a precision on the prefactors. At large bias voltages, the current enlarges the typical width of the Kondo resonance, which produces the robustness of the phase shift. Using this form of Γ , with a Kondo temperature $T_K \approx 550$ mK and a position $\epsilon_0 \sim k_B T_K$ of the Kondo resonance, we can explain (almost quantitatively) the experimental observations; see Figs. 3(b), 3(d), and 3(f). The low-bias features in the amplitude signal can also be accounted for by our model. Note that the low-bias anomaly observed in the phase response in Fig. 3(a) is beyond the scope of our present Fermi-liquid analysis. Increasing the bias voltage such that $eV_{sd} > k_B T_K$, the logarithmic renormalization factors in Eq. (4.1) then contribute to maintain important dissipation effects until $\Gamma > e|V_{sd}|$. Using results of Fig. 10 of Appendix C and Eqs. (4.1) above, then we predict that the π -phase shift in the reflected light signal subsists until $e|V_{sd}| \sim 10k_B T_K$, which means roughly the charging energy E_C . For larger bias voltages, when $e|V_{sd}| \gg \Gamma$, we check that $\text{Im}\Pi^R(\omega_0^*) \sim 0$, justifying that the phase shift then smoothly drops to zero in the very high-bias regime.

A similar renormalization group argument can be formulated as a function of temperature showing that the π -phase shift should indeed disappear when $T \sim T_K$. A detailed microscopic model of the experimental set up, the construction of the effective $SU(4)$ Kondo model and its coupling to the photon field together with few relevant calculations are included

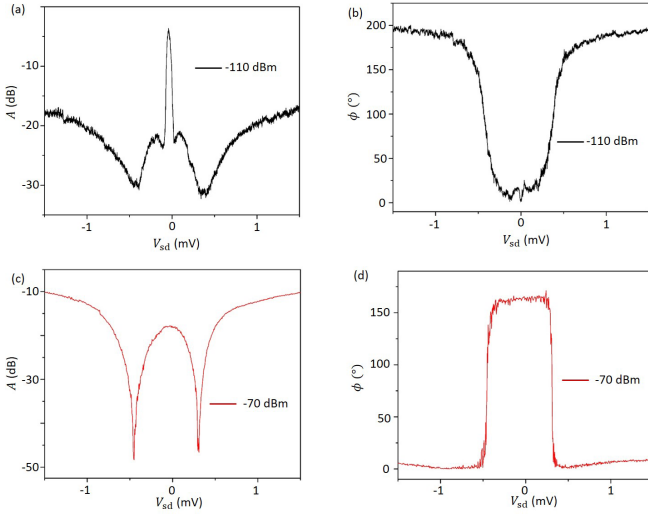


FIG. 7. Amplitude (a) and phase (b) response as functions of the bias voltage for the point D. Same results when increasing the microwave power (c) and (d).

in Appendix C, where we also show that a bias-independent resonant level model (modeling the two degenerate charge states) would not explain the data, showing that many-body effects through the formation of a Kondo resonance cannot be ignored.

V. COULOMB BLOCKADE REGIME AND MICROWAVE POWER

We now study the power (P) dependence of the resonator response as a function of the bias voltage at point D. We verify that the electron transport at this point D in the charge stability diagram is now blocked at low energy. Our goal is to demonstrate experimentally here that the effect of the microwave power on the light response plays a similar role as moving along a line relating the point D to a charge degeneracy point, and therefore restoring the same light responses as for point A. For the theoretical description, we will apply the two unitary transformations in Eq. (B3) and Eq. (B8) of Appendix B.

Fixing the driving frequency at resonance $\omega = \omega_0^*(V_{sd})$, we show the amplitude response [Figs. 7(a) and 7(c)] and the phase response [Figs. 7(b) and 7(d)] for two different values of the power. Figures 7(a) and 7(b) show the phase and amplitude response at weak power. A phase shift is confirmed from bias voltage $V_{sd} = 0$ to $V_{sd} \simeq \pm 0.5$ mV. The amplitude sharply goes down for about -15 dB from $V_{sd} = 0$ to $V_{sd} \simeq \pm 0.1$ mV, and two side peaks appear around $V_{sd} \simeq \pm 0.15$ mV. Then, it continues to go down and two dips appear around $V_{sd} \simeq \pm 0.4$ mV, which are again consistent with the charging energy E_C of the quantum dots measured by the Coulomb diamond. At small V_{sd} , this confirms that the Coulomb blockade phenomenon pins the charge fluctuations on the DQD and as a result the photon field is weakly affected by the matter. When the bias voltage increases and compensates the charging energy, there is a revival of charge fluctuations on the DQD. It is important to note that the cavity is only coupled to the orbital degree of freedom, leading to a phase of zero when

$V_{sd} \rightarrow 0$. As a result, it is not sensitive to an eventual spin Kondo effect where the spin and orbital degrees of freedom are decoupled (resulting from the system composed of the left dot and the left lead alone). A more refined theoretical analysis would be necessary to describe quantitatively the crossover with voltage and to include the charging energy effects.

We see that the phase response is drastically modified as the power changes. At high power the amplitude and phase response are close to the ones obtained at point A. This observation can be explained by the fact that the photonic interaction acts as an artificial chemical potential at high drive powers, bringing the system from the Coulomb blockade regime to the resonant regime. More precisely, in the large drive regime, we can decompose the photon field as the sum of its mean value plus quantum fluctuations. This leads to a rewriting of the photon annihilation operator as $a = \langle a \rangle + \tilde{a}$. The first part $\langle a \rangle$ is determined by the strength of the drive field and the damping rate, and we suppose that steady state of the cavity is a coherent state. The constant semi-classical part of the drive $\langle a + a^\dagger \rangle$ acts as a chemical potential on the Left dot. Following Ref. [2] the chemical potentials of the two dots μ_L and μ_R read as a function of the number of electrons on the dots (N_L and N_R),

$$\mu_L(N_L, N_R) = \left(N_L - \frac{1}{2} - \lambda \langle a + a^\dagger \rangle \right) E_{C_L} + N_R E_{C_m} - \frac{1}{|e|} (C_{gL} V_{LP} E_{C_L} + C_{gR} V_{RP} E_{C_m}) \quad (5.1)$$

$$\mu_R(N_L, N_R) = \left(N_R - \frac{1}{2} \right) E_{C_R} + N_L E_{C_m} - \frac{1}{|e|} (C_{gL} V_{LP} E_{C_m} + C_{gR} V_{RP} E_{C_R}), \quad (5.2)$$

where E_{C_j} is the charging energy of the individual dot j , E_{C_m} is the electrostatic coupling energy, C_j (C_{g_j}) is the capacitance coupling the dot j to the neighboring lead (gate), and C_m is the capacitance, which couples the dots together. The Left and Right gate voltages are denoted by V_{LP} and V_{RP} . The effect of the driving can be absorbed into the definition of new gates voltages V'_{LP} and V'_{RP} ,

$$V'_{LP} = V_{LP} - \frac{\lambda \langle a + a^\dagger \rangle |e|}{C_{gL} (E_{C_L} - \frac{E_{C_m}^2}{E_{C_R}})} \quad (5.3)$$

$$V'_{RP} = V_{RP} - \frac{\lambda \langle a + a^\dagger \rangle |e|}{C_{gR} (E_{C_m} - \frac{E_{C_L} E_{C_R}}{E_{C_m}})} \quad (5.4)$$

Driving the system at high power allows to move the state of the system on the honeycomb phase diagram along a line characterized by the Eqs. (5.3) and (5.4). This corresponds to

$$\frac{\delta V_{RP}}{\delta V_{LP}} = \frac{C_{gL} E_{C_m}}{C_{gR} E_{C_R}}. \quad (5.5)$$

Such a line has a slope, which is the opposite of the line of degeneracy between the states $(N, M - 1)$ and (N, M) (the line where lies the point B).

We can see from Fig. 8 that driving the cavity may bring the system at resonance. We can estimate the input power that allows to make this transition from the Coulomb blockade

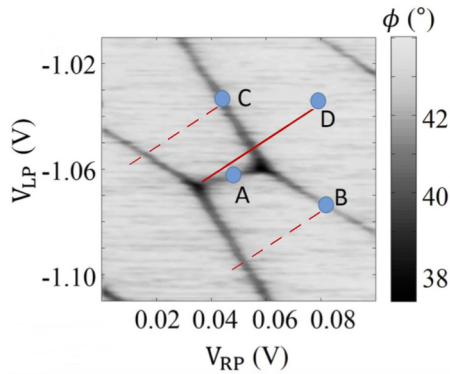


FIG. 8. Effect of the driving on the state of the system. The full-red line shows the shift in the phase diagram induced by the drive at point D.

regime to the resonant regime. In the steady state, the input-output theory allows to relate the drive power to the number of photons in the cavity and ultimately to $\langle a + a^\dagger \rangle$. We have $P = (\hbar\omega\eta/4)\langle a^\dagger a \rangle$, where η is the decay rate of the photons in the leads (assumed to be independent over the range of frequencies relevant to the cavity in the Markov approximation). If we suppose that the steady state of the cavity is a coherent state, we have

$$\langle a^\dagger + a \rangle \simeq \sqrt{\frac{P}{\hbar\omega\eta}}. \quad (5.6)$$

We conclude that, at a mean field level, driving the system indeed allows to move the state of the system on the honeycomb phase diagram, as the mean field contribution can shift the left chemical potential. In the steady state, the input-output theory allows to relate the drive power to the number of photons in the cavity and ultimately to $\langle a + a^\dagger \rangle$ if we suppose that the steady state of the cavity is a coherent state. Following Ref. [38], we have $P = \hbar\omega\frac{\eta}{4}\langle a^\dagger a \rangle$, where η is the frequency-independent decay rate of the photons in the leads. For a coherent state in the cavity this allows to write $\langle a^\dagger + a \rangle \simeq \sqrt{P/(\hbar\omega\eta)}$. We can then estimate the critical power P_c needed to compensate E_C . We have $E_C = 0.4$ meV, $\omega = 7$ GHz, and we take $\lambda \simeq 0.15$ GHz and $\eta \simeq 0.1$ GHz. This finally gives $P_c \simeq 10^{-10}$ W = -70 dBm, which is consistent with the experimental observations. We note that the high-power responses at small biases differ slightly from those at point A. This may be linked to additional nonequilibrium effects arising at high power.

VI. CONCLUSION

We have shown how the Kondo resonance can interact with the microwave photon field, producing a π -phase shift of light at low temperatures. The microwave frequency is adjusted carefully at the many-body light resonance frequency corresponding to the minimum of the amplitude of the light response, revealing important many-body dissipation effects. Applying the Korringa-Shiba relation of quantum impurity Fermi liquid Kondo models and renormalization group arguments to include bias voltage effects in the Kondo resonance and in the spectral function on the DQD, then we have shown

how such a π -phase shift of light can subsist until energies larger than the Kondo scale, roughly around the charging energy of the mesoscopic system. Our findings are also in agreement with a many-body electronic spectral function, which is located above the Fermi energy according to an $SU(4)$ symmetry in the Fermi-liquid description. It is important to highlight here that the π -phase shift is an intrinsic property of Fermi liquid impurity models and could also be observed for Kondo systems with $SU(2)$ symmetry assuming the light is at the right resonance condition. Our paper shows how microwave spectroscopy can probe the dynamical properties of the correlated electron system when the microwave frequency is synchronized with the typical frequency scale associated with the correlated phenomenon. Similar to three-lead or four-lead geometries [8], the microwave resonator allows then to study important features of the spectral function on the mesoscopic system. We have quantitatively described photon-electron many-body effects in our device and our work opens up new possibilities for fundamental and practical applications in many-body light-matter systems. An analogous microwave signature of charge Kondo effect could be observed in a hybrid metal-semiconductor implementation of a single-electron transistor [55]. Light may also give further information on the microwave response of a two-impurity model in the double-dot geometries [56]. We also anticipate that light may probe topological phenomena associated to the occurrence of π Berry phases [57].

ACKNOWLEDGMENTS

We acknowledge discussions with Camille Aron, Sebastian Diehl, Serge Florens, Loïc Herviou, Takis Kontos, Julian Legendre, Vladimir Manucharyan, Christophe Mora, Nicolas Roch and Achim Rosch on related hybrid systems. We thank Olesia Dmytruk, Pascal Simon, Mircea Trif, and Ryosuke Yoshii for useful comments. This work was supported by the National Key Research and Development Program of China (Grants No. 2016YFA0301700 and No. 2018YFA0306102), the National Natural Science Foundation of China (Grants No. 11625419, No. 61704164, No. 91836102, No. 61674132, No. 11674300, and No. 11575172), and the Anhui Initiative in Quantum Information Technologies (Grant No. AHY080000). This research has also benefited from support from the DOE, under the grant DE-FG02-08ER46541. This work is partially supported by ANR BOCA. This work was partially carried out at the USTC Center for Micro and Nanoscale Research and Fabrication.

APPENDIX A: SAMPLES

The samples are fabricated as follows. First, we mechanically exfoliated the graphene from its bulk, KISH graphite (Kyocera. Inc), to an undoped silicon chip with 285 nm oxide. In this experiment, we need two pieces of few-layer graphene with proper distance between 20 to 80 μm , and we selected those that met this requirement. Second, electron beam lithography (EBL) was employed several times, starting with the fabrication of alignment marks, then plasma-etching masks and electrode patterns. The EBL resists used were PMMA 950k A4 for the first step and double-layered

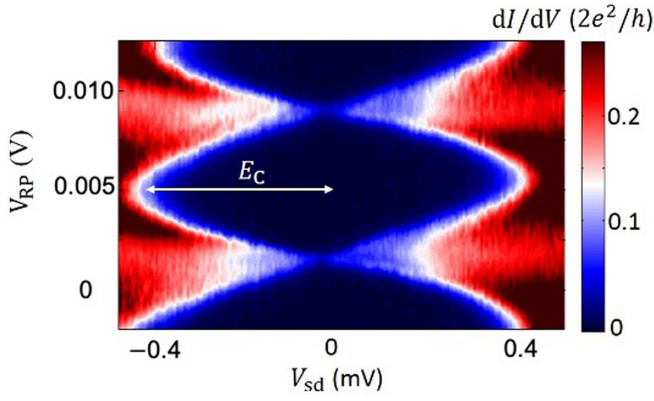


FIG. 9. Coulomb diamond of the quantum dot measured by transport experiment and revealing the charging energy E_C . We use a single-charging energy in agreement with previous measurements [48,49]. The charging energies of the two dots are measured to be almost identical, and we find that the mutual capacitance is of the order of the single-dot capacitances. All microwave and dc transport measurements support this argument.

PMMA 950k A2 for the latter two steps. We developed the submicrometer patterns under 0 to establish a better control of the device specifications. Through etching out all the undesired part of the graphene sheet to realize the designed device, we strove for the all-metal-side-gated configuration as described in Ref. [58], to avoid unstable gate terminals. This etching was carried out by inductively-coupled plasma (ICP), using a 4:1 gas mixture of oxygen to argon. For marks and electrodes, we deposited 5 nm Ti and 45 nm Au with an electron-beam evaporator. Finally, the resonator was fabricated by optical lithography followed by metal deposition in a thermal evaporator. The metal used was 200-nm-thick Al.

The microwave response was measured using a network analyzer (NA). The input and output ports of the NA were connected to the resonator via a circulator and a 180 degree hybrid, which splits the reflected signal back to the NA. Two 30 dB attenuators were connected between the NA output port and the circulator, reducing the power applied to the resonator down to lower than -130 dBm. The reflected signal was amplified first at 4 K and then at room temperature, producing an additional gain of 60 dB, and an isolator was used to prevent noise from the amplifiers and the environment from reaching the sample. The direct transport current was amplified by a low-noise current pre-amplifier, before being measured by a digital multimeter.

The Coulomb diamond can be measured by transport experiment and revealing the charging energy E_C , as shown in Fig. 9. We emphasize here that gate lever arms are $\sim 10\%$ by using a typical calculation method [59], such that we obtain a charging energy $E_C \sim 0.4$ meV.

APPENDIX B: GRAPHENE DQD AND LIGHT-MATTER COUPLING

The Hamiltonian of a double dot setup takes the form [2,60] $H_1 = H_L + H_R + H_D + H_T$, where

$$H_{l=L,R} = \sum_{k\sigma} (\epsilon_k + V_l) c_{k\sigma l}^\dagger c_{k\sigma l}$$

$$\begin{aligned} H_D &= \sum_{l=L,R} \sum_{p_l, \sigma} (\epsilon_{p_l} d_{p_l \sigma}^\dagger d_{p_l \sigma}) + \gamma_L n_L (n_L - 1) \\ &\quad + \gamma_R n_R (n_R - 1) + \gamma_M n_L n_R \\ H_T &= \sum_{l=L,R} \sum_{k, \sigma} \sum_{p_l} (t_{kn_l} c_{k\sigma l}^\dagger d_{p_l \sigma} + \text{H.c.}) \\ &\quad + \sum_{p_L p_R \sigma} (t_{p_L p_R} d_{p_L \sigma}^\dagger d_{p_R \sigma} + \text{H.c.}). \end{aligned} \quad (\text{B1})$$

The first line describes the electrons in the Left (L) and Right (R) leads (respectively source and drain). $c_{k\sigma l}$ ($c_{k\sigma l}^\dagger$) is the annihilation (creation) operator of an electron of spin σ and energy ϵ_k and in the lead l , on which we apply a voltage V_l . $V_{sd} = V_L - V_R$ denotes the bias voltage applied across the device. The term H_D describes the two dots: $d_{p_l \sigma}$ ($d_{p_l \sigma}^\dagger$) is the annihilation (creation) operator of an electron of spin σ in the dot $l = L, R$ and at the energy level p_l . Here the coefficients γ are functions of the capacitances of the tunnel junctions and $n_l = \sum_{p_l, \sigma} d_{p_l \sigma}^\dagger d_{p_l \sigma}$ denotes the number of electrons in the dot l . The part H_T accounts for lead-dot and inter-dots tunneling events.

The model presented here can be explicitly refined to incorporate the precise geometry of the graphene lattice (leads) [61], and consider the two sublattices A and B of the honeycomb lattice. Since the DQD size (of the order of a few hundred nanometers) is much larger than the atomic distance between neighboring sites in graphene, we can assume that the tunneling probability from the leads in a given quantum dot is independent of the sublattice. In Eq. (B1), H_T can then be written as a function of the symmetric operator $1/\sqrt{2}(c_{k\sigma lA} + c_{k\sigma lB})$ in a given lead l . The kinetic term leading to a Dirac type linear dispersion can also be diagonalized in this basis if we assume a symmetric configuration for the A and B sites with respect to the direction of the tunneling. The use of either open or periodic boundary conditions in the orthogonal direction then lead to a one-dimensional kinetic Hamiltonian along the direction of the tunneling, which is diagonal in this symmetric/antisymmetric basis [62,63]. With these arguments, Hamiltonian (B1) remains valid with the electronic operators referring to the symmetric operator (between sublattices A and B) in a given lead. Notice that k formally refers to the wave vector along the direction of propagation across the mesoscopic system.

The interaction between microwave photons and the electronic degrees of freedom is often approximated by a dipolar coupling [48,64–66]. The authors provided a general description in the case of a nanocircuit embedded inside the cavity. In our setup, the electrons of the left lead couple to the electric field at the extremity of a superconducting microwave resonator, as shown in Fig. 1(c). The total Hamiltonian of the coupled light-matter system becomes $H = H_1 + H_2$ with

$$H_2 = \hbar \omega_0 a^\dagger a + \frac{\lambda}{\sqrt{2}} (a + a^\dagger) \left(\sum_{k\sigma} c_{k\sigma L}^\dagger c_{k\sigma L} \right). \quad (\text{B2})$$

To study the effect of the light degrees of freedom onto the Kondo model, we apply one first unitary transformation on

the Hamiltonian H and define $H' = U^\dagger H U$. We have

$$U = \exp \left[i\theta \left(\sum_{k\sigma} c_{k\sigma L}^\dagger c_{k\sigma L} \right) \right], \quad (\text{B3})$$

where $\theta = \frac{\lambda(a-a^\dagger)}{i\sqrt{2}\hbar\omega_0}$. We can compute the transformed Hamiltonian H' thanks to the Baker-Campbell-Hausdorff formula $e^X Y e^{-X} = Y + [X, Y] + \frac{1}{2!}[X, [X, Y]] + \frac{1}{3!}[X, [X, [X, Y]]] + \dots$. We then get

$$U^\dagger c_{k\sigma l} U = c_{k\sigma l} e^{i\theta} \quad (\text{B4})$$

$$U^\dagger (\hbar\omega_0 a^\dagger a) U = -\frac{\lambda}{\sqrt{2}}(a + a^\dagger) \left(\sum_{k\sigma} c_{k\sigma L}^\dagger c_{k\sigma L} \right) \quad (\text{B5})$$

$$U^\dagger \left(\lambda(a + a^\dagger) \left(\sum_{k\sigma} c_{k\sigma L}^\dagger c_{k\sigma L} \right) \right) U = \frac{\lambda^2}{\hbar\omega_0} \left(\sum_{k\sigma} c_{k\sigma L}^\dagger c_{k\sigma L} \right)^2. \quad (\text{B6})$$

Assuming small fluctuations concerning the total number of conduction electrons, the right hand side of Eq. (B6) is almost a constant, so that the resulting Hamiltonian reads $H' = H_L + H_R + H_D + H'_T + \hbar\omega_0 a^\dagger a$, where we have

$$\begin{aligned} H'_T = & \sum_{k\sigma} \sum_{pL} (t_{kpL} c_{k\sigma L}^\dagger d_{pL\sigma} e^{-i\theta} + h.c.) \\ & + \sum_{k\sigma} \sum_{pR} (t_{kpR} c_{k\sigma R}^\dagger d_{pR\sigma} + H.c.) \\ & + \sum_{pLpR\sigma} (t_{pLpR} d_{pL\sigma}^\dagger d_{pR\sigma} + H.c.). \end{aligned} \quad (\text{B7})$$

This unitary transformation has suppressed the explicit coupling between the source lead and the resonator. The tunneling terms from the source lead to the left dot have moreover acquired a phase, which depends on the state of the resonator.

We apply then a second unitary transformation $\tilde{H} = V^\dagger H' V$, with

$$V = \exp \left[i\theta \left(\sum_{pL\sigma} d_{pL\sigma}^\dagger d_{pL\sigma} \right) \right]. \quad (\text{B8})$$

After similar calculations, the resulting Hamiltonian reads $\tilde{H} = H_s + H_d + \tilde{H}_D + \tilde{H}_T + \hbar\omega_0 a^\dagger a$, where we have

$$\begin{aligned} \tilde{H}_D = & H_D - \frac{\lambda}{\sqrt{2}}(a + a^\dagger) \left(\sum_{pL\sigma} d_{pL\sigma}^\dagger d_{pL\sigma} \right) \\ \tilde{H}_T = & \sum_{l=L,R} \sum_{k\sigma} \sum_{p_l} (t_{kp_l} c_{k\sigma l}^\dagger d_{p_l\sigma} + H.c.) \\ & + \sum_{pLpR\sigma} (t_{pLpR} d_{pL\sigma}^\dagger d_{pR\sigma} e^{-i\theta} + H.c.). \end{aligned} \quad (\text{B9})$$

In this final form, the mode of the resonator is coupled to the energy levels of the Left dot. Additionally, the tunneling term between the dots has acquired a phase, which depends on the \hat{p} operator of the mode. In the article, the \hat{x} field (describing the quantization of the electric field in the cavity) is related to $(a + a^\dagger)$.

We can characterize the effect of the DQD on the resonator at point A by measuring the amplitude response as a function

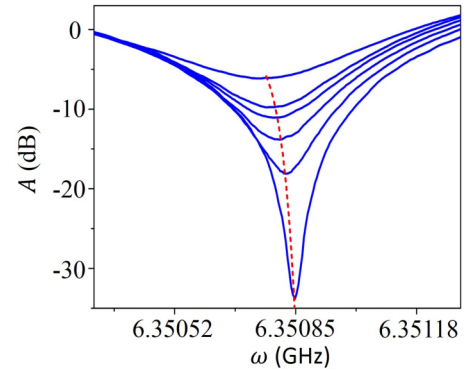


FIG. 10. Amplitude response A as a function of the driving frequency ω , for various bias voltages (0, 0.5, 0.6, 0.7, 0.8, 1 mV) at point A. The red dashed line shows the fitted resonance frequency, shifted by the electron transport.

of the driving frequency, for various bias voltages, as shown in Fig. 10. The coupling to the electronic system leads to a renormalization of the bare resonator frequency ω_0 to a voltage-dependent value $\omega_0^*(V_{sd})$, which can be seen in the amplitude response of the cavity (and associated with the red dashed line in Fig. 10) [37].

APPENDIX C: DESCRIPTION OF THE $SU(4)$ KONDO MODEL

The low-energy theory of the electronic degrees of freedom at point A can be built in perturbation theory, by restricting the electron dynamics on the dot to the two allowed states $(N-1, M)$ and $(N, M-1)$. We can then introduce a pseudospin degree of freedom \vec{T} to describe the two charge states by analogy with a double-well problem, assuming the limit of small quantum dots [25]. The spin \vec{S} of electrons will couple to the pseudospin degrees of freedom when taking into account second-order tunneling processes.

1. $SU(4)$ Kondo Model

As a result of second-order tunneling processes, the electron leads are coupled through the Hamiltonian $H_1 = H_{\text{kin}} + H_{\text{kondo}} + H_{\text{assist}} + H_{\text{orbital}}$ [25]. Here, H_{kin} represents the kinetic energy in the two leads. Second-order tunneling processes are classified through purely Kondo terms involving spin flips, orbital contributions changing the lead index from say $l = L$ (Left) to $l = R$ (Right) and flipping the charge state on the DQD, and assisted tunneling processes entangling the charge and spin:

$$\begin{aligned} H_{\text{Kondo}} + H_{\text{assist}} = & \frac{J}{2} \vec{S} \psi^\dagger \vec{\sigma} \psi + Q_z T^z \vec{S} \psi^\dagger \tau^z \vec{\sigma} \psi \\ & + Q_\perp (T^+ \vec{S} \psi^\dagger \tau^- \vec{\sigma} \psi + H.c.) \\ H_{\text{orbital}} = & \frac{1}{2} (V_z T^z \psi^\dagger \tau^z \psi + V_\perp (T^+ \psi^\dagger \tau^- \psi \\ & + H.c.)), \end{aligned} \quad (\text{C1})$$

where $\psi_{\sigma l}$ is the Fourier transform of $c_{k\sigma l}$ which refers to an electron operator with spin σ in lead l . Here, \vec{S} corresponds to the spin operator of the electron delocalized on the DQD,

\vec{T} to the pseudospin associated to the charge dynamics on the DQD, $\vec{\sigma}$ and $\vec{\tau}$ act on the spin space and orbital (lead) space of the electron operators. The couplings above can be written in terms of the tunneling rate to the right/left lead Γ_{\pm} and the charging energy E_c of the DQD, respectively, as [25] $J = Q_z = (\Gamma_+ + \Gamma_-)/4E_c$, $Q_{\perp} = V_{\perp} = \sqrt{\Gamma_+\Gamma_-}/E_c$.

To generalize this Hamiltonian in graphene, we assume that an electron in graphene leads, has an equal probability to hop onto the DQD when belonging to sublattice A or sublattice B . In this sense, the c -operator corresponds to the symmetric combination of A and B sublattice electron operators in graphene. A small asymmetry between these tunneling elements (smaller than the Kondo energy scale) should not affect the results in the article. We argue that a small geometrical asymmetry of the tunneling between the two graphene sublattices is unimportant, as the symmetric term would dominate in the renormalization procedure of Ref. [25].

It should also be noted that the tunneling term between the two dots also involve the phase (operator) θ after the unitary transformation done above. Therefore, the coupling between the two dots gives rise to an orbital magnetic field $t' \exp(-i\theta)T^+ + \text{H.c.}$. When focusing on dc transport we redefine $t' \rightarrow t' \exp(-i\theta)$. The important point is that, in contrast to a macroscopic environment, which may suppress the dc conductance [26], the coupling with a single-mode resonator should not affect the transmission between the two dots in the limit of zero frequency. The main process for dc conductance should not be accompanied by the emission of a (single) photon.

2. Fermi liquid picture

The starting point of our analysis is that the system flows to a Kondo-Fermi-liquid fixed point [25,27–29,50,67,68], which is quite robust to (charge) noise effects [26]. Experiments have reported the possible occurrence of an emergent $SU(4)$ symmetry at the low-energy fixed point, in similar geometries, due to the entanglement between spin and orbital degrees of freedom [4,5,7,39,69]. The remarkable fact is that the bare parameters of the model are replaced by a single parameter describing the low-energy fixed point, namely the Kondo energy scale $k_B T_K$. In this description the spectral function of the DQD can be modeled by an effective resonant level model [28], associated with spinless fermionic operators d and d^\dagger defined in the article and describing the two macroscopic charge states on the DQD. These operators d and d^\dagger are defined in correspondence with the processes involving the orbital operators T^- and T^+ , respectively. This spinless description is legitimate as the two spin components add up in the conductance, and the cavity only couples to the orbital degree of freedom. We highlight that even though we describe the effective resonant level with spinless operators, the spin of the electrons is a highly relevant quantity: the joint effect of the orbital and spin degrees of freedom lead to the $SU(4)$ Kondo resonance at ϵ_0 of the order of $k_B T_K$, above the Fermi surface.

In this regime, the system can then be treated by analogy with the case of one single dot studied in Ref. [37], the only difference being that the position ϵ_0 and the width $\Gamma(V_{sd})$ of the electronic level are determined by the $SU(4)$ fixed point,

leading to a the spectral function of the form:

$$\rho(\omega) = \frac{1}{\pi} \frac{\Gamma(V_{sd})}{(\hbar\omega - \epsilon_0)^2 + \Gamma(V_{sd})^2}, \quad (\text{C2})$$

where the position of the resonance ϵ_0 is of the order of $k_B T_K$ [27,28]. We take a bias dependent width $\Gamma(V_{sd})$ for the pseudofermion d to account for dissipation effects at large voltages, see below.

3. Voltage dependent level width

We estimate perturbatively the decoherence rate Γ at large bias voltages, adopting the pseudofermion d and d^\dagger resonance description (related to the orbital degrees of freedom T^- and T^+ , respectively). The decoherence channels on the Kondo effect at large bias voltages will be provided by the terms involving T^- and T^+ , namely V_{\perp} and Q_{\perp} . It is quite straightforward to compute the imaginary-part of the self energy of the d fermion to second order in V_{\perp} and Q_{\perp} .

For the V_{\perp} channel, by analogy with the $SU(2)$ Kondo effect [54], we find

$$\Gamma_1 = 2 \int d\omega' V_{\perp}^2(\omega') f_{\omega' - \mu_L}(1 - f_{\omega' - \mu_R}). \quad (\text{C3})$$

To simplify, here we set $\hbar = 1$. In this expression, the factor 2 comes from the two spin polarizations of an electron, f is the Fermi distribution and μ_L and μ_R are the chemical potentials in the two leads. Since we consider high-frequency scales of the order of $\omega' \sim eV_{sd}$ or short time scales smaller than $1/(k_B T_K)$, for the pseudofermion d evolution in time, we have replaced $\exp(-i\epsilon_0 t)$ by one since $\epsilon_0 \sim T_K$.

In a similar way, for the Q_{\perp} channel, we find

$$\Gamma_2 = 4 \int d\omega' Q_{\perp}^2(\omega') f_{\omega' - \mu_L}(1 - f_{\omega' - \mu_R}). \quad (\text{C4})$$

The factor 4 encodes all the spin possibilities allowed by the Q_{\perp} channel. The total decoherence rate is $\Gamma = \Gamma_1 + \Gamma_2$.

To find Eq. (4.1) at large bias voltages in the main text we proceed as follows. First, based on the renormalization group equations of the $SU(4)$ Kondo model [67], we can approximate $V_{\perp}(\omega) \sim Q_{\perp}(\omega) = J(\omega)$. This leads to the following equation for $\omega' \approx eV_{sd} \gg k_B T_K$:

$$\frac{1}{4J(\omega')} \approx \log\left(\frac{eV_{sd}}{k_B T_K}\right), \quad (\text{C5})$$

where we have used the definition of the $SU(4)$ Kondo energy scale

$$k_B T_K = D \exp(-1/4J(D)), \quad (\text{C6})$$

where D is an ultraviolet cutoff, essentially E_c in the present case. Extending this form of solutions in all the frequency window set by eV_{sd} then leads to

$$\begin{aligned} \Gamma &= k_B T_K \text{ for } eV_{sd} \ll k_B T_K, \\ \Gamma &\sim \frac{6}{16} \frac{eV_{sd}}{\ln^2(eV_{sd}/k_B T_K)} \text{ for } eV_{sd} \gg k_B T_K, \end{aligned} \quad (\text{C7})$$

by analogy with the $SU(2)$ Kondo effect [54].

At large bias voltages, the current produces dissipation and decoherence effects on the Kondo resonance. A polynomial interpolation is performed between small and large biases, and

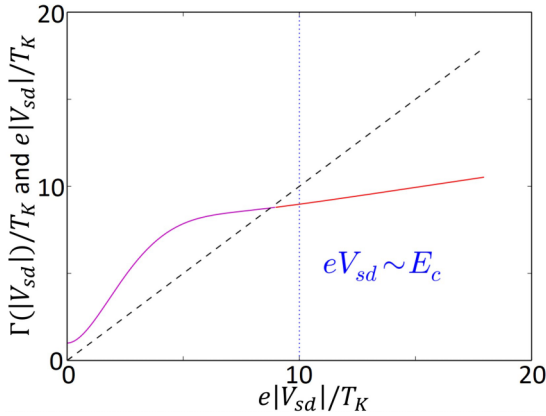


FIG. 11. Evolution of Γ/T_K with respect to eV_{sd}/T_K (here $k_B = 1$). At low-bias voltages, we have $\Gamma/T_K \sim 1$, while $\Gamma \sim V_{sd}/[\ln(V_{sd}/T_K)]^2$ for large biases $eV_{sd}/T_K \gg 1$ (full red line). This expression is valid asymptotically and for $\Gamma < V_{sd}$ [54]. We use a polynomial (here degree 6) interpolation between these two limits (full magenta line). The vertical dotted blue line shows the value of the charging energy E_C .

the resulting behavior is shown in Fig. 11. As can be seen in this figure, $(\Gamma(V_{sd}) - eV_{sd})$ (given by the space between the magenta line and the dashed black line) initially decreases until $e|V_{sd}| \sim k_B T_K$, which is responsible for the low-energy features in the amplitude. For $e|V_{sd}| \geq k_B T_K$, we still observe a robust π phase in the reflected signal. At $e|V_{sd}|/k_B T_K \sim 10$, the quantity $\Gamma(V_{sd})$ becomes smaller than V_{sd} , leading to a drop of the phase shift from π to 0. Above $e|V_{sd}| \sim E_C$ (vertical dotted blue line) the model is not valid as we should take into account other energy levels.

As T_K can be estimated from dc transport measurements (see Fig. 2 in the article), we only use one fitting parameter to obtain Fig. 11: the proportionality coefficient on the right hand side of Eq. (C7); we also check that changing the dissipation strength α does not affect much the results (in the weak-dissipation regime). This particular evolution of the

resonance width Γ determines the electron-induced photon lifetime, $\text{Im}\Pi^R(\omega_0^*(V_{sd}))$. Using the Fermi liquid picture then gives [37]

$$\begin{aligned} \text{Im}\Pi^R(\omega_0^*) &= \lambda^2 f_\Gamma(\omega_0^*) \sum_{\alpha, a=\pm} \alpha \arctan\left(\frac{\mu_a - \epsilon_0 + \alpha \hbar \omega_0^*}{\Gamma}\right) \\ &+ \lambda^2 f_\Gamma(\omega_0^*) \sum_{\alpha, a=\pm} \frac{\Gamma}{\omega_0^*} \ln\left(\frac{(\mu_a - \epsilon_0 + \alpha \hbar \omega_0^*)^2 + \Gamma^2}{(\mu_a - \epsilon_0)^2 + \Gamma^2}\right) \end{aligned} \quad (\text{C8})$$

where $f_\Gamma(\omega_0^*) = \Gamma/(4\pi^2\Gamma^2 + \pi^2\hbar^2\omega_0^{*2})$. In addition, $\mu_a = aeV_{sd}/2$ are the chemical potentials associated with each lead, where formally $a = +1$ for left (L) lead and $a = -1$ for right (R) lead. Formally, this form of $\text{Im}\Pi^R(\omega_0^*)$ is obtained by considering the limit $|t'|\lambda/\omega_0^* \ll \lambda$. The phase and amplitude of transmitted photons are then directly obtained from $\text{Im}\Pi^R(\omega_0^*)$ in the article. Corresponding results are shown in Fig. 3.

4. Comparison with a non-interacting Resonant level Model

We now argue that the experimental results in Fig. 3 are not compatible with a simple analysis of the electronic system (biased leads plus double quantum dots) based on a resonant level model as was done in Ref. [37]. Indeed in this picture the electronic lifetime would be essentially bias independent and set by the width of the resonance Γ . Results of Fig. 3 in the main text would then suggest $\Gamma \simeq E_C = 0.4$ meV. Such a large value of Γ seems unphysical (in the context of a DQD weakly coupled to graphene leads). Moreover, the electronic levels in the Coulomb diamond would not be well defined. This is also in contradiction with the presence of two distinct energy scales in the amplitude of the reflected microwave signal. In contrast, we attribute the robustness of the π phase and the low-bias features of the amplitude response to a formation of a bound state between light and matter in the Kondo regime, leading to a strong voltage dependence for Γ .

-
- [1] D. Goldhaber-Gordon, D. H. Shtrikman, D. Mahalu, D. Abusch-Magder, U. Meirav, and M. A. Kastner, *Nature (London)* **391**, 156 (1998).
- [2] W. G. van der Wiel, S. D. Franceschi, J. M. Elzerman, T. Fujisawa, S. Tarucha, and L. P. Kouwenhoven, *Rev. Mod. Phys.* **75**, 1 (2002).
- [3] L. Kouwenhoven and L. Glazman, *Phys. World* **14**, 33 (2001).
- [4] P. Jarillo-Herrero, J. Kong, H. S. van der Zant, C. Dekker, L. P. Kouwenhoven, and S. D. Franceschi, *Nature (London)* **434**, 484 (2005).
- [5] A. Makarovski, J. Liu, and G. Finkelstein, *Phys. Rev. Lett.* **99**, 066801 (2007).
- [6] T. Hata, R. Delagrange, T. Arakawa, S. Lee, R. Deblock, H. Bouchiat, K. Kobayashi, and M. Ferrier, *Phys. Rev. Lett.* **121**, 247703 (2018).
- [7] A. J. Keller, S. Amasha, I. Weymann, C. P. Moca, I. G. Rau, J. A. Katine, H. Shtrikman, G. Zarand, and D. Goldhaber-Gordon, *Nat. Phys.* **10**, 145 (2014).
- [8] R. Leturcq, L. Schmid, K. Ensslin, Y. Meir, D. C. Driscoll, and A. C. Gossard, *Phys. Rev. Lett.* **95**, 126603 (2005).
- [9] Y. Ji, M. Heiblum, D. Sprinzak, D. Mahalu, and H. Shtrikman, *Science* **290**, 779 (2000).
- [10] M. Zaffalon, A. Bid, M. Heiblum, D. Mahalu, and V. Umansky, *Phys. Rev. Lett.* **100**, 226601 (2008).
- [11] M. Sato, H. Aikawa, K. Kobayashi, S. Katsumoto, and Y. Iye, *Phys. Rev. Lett.* **95**, 066801 (2005).
- [12] S. Takada, C. Bäuerle, Y. Yamamoto, K. Watanabe, S. Hermelin, T. Meunier, A. Alex, A. Weichselbaum, J. von Delft, A. Ludwig, A. D. Wieck, and S. Tarucha, *Phys. Rev. Lett.* **113**, 126601 (2014).
- [13] A. Dousse, L. Lanco, J. J. Suffczynski, E. Semenova, A. Miard, A. Lemaitre, I. Sagnes, C. Roblin, J. Bloch, and P. Senellart, *Phys. Rev. Lett.* **101**, 267404 (2008).
- [14] M. R. Delbecq, V. Schmitt, F. D. Parmentier, N. Roch, J. J. Viennot, G. Fève, B. Huard, C. Mora, A. Cottet, and T. Kontos, *Phys. Rev. Lett.* **107**, 256804 (2011).

- [15] T. Frey, P. J. Leek, M. Beck, A. Blais, T. Ihn, K. Ensslin, and A. Wallraff, *Phys. Rev. Lett.* **108**, 046807 (2012).
- [16] M. M. Desjardins, J. J. Viennot, M. C. Dartiailh, L. E. Bruhat, M. R. Delbecq, M. Lee, M. S. Choi, A. Cottet, and T. Kontos, *Nature (London)* **545**, 71 (2017).
- [17] S. Léger, J. Puertas-Martinez, K. Bharadjwaj, R. Dassoneville, D. J., F. Foroughi, V. Michalkov, L. Planat, O. Buisson, C. Naud, W. Hasch-Guichard *et al.*, *Nat. Commun.* **10**, 5259 (2019).
- [18] P. Forn-Díaz, J. J. Garcia-Ripoll, B. Peropadre, J. L. Orgiazzi, M. A. Yurtalan, R. Belyansky, C. M. Wilson, and A. Lupascu, *Nat. Phys.* **13**, 39 (2016).
- [19] L. Magazzù, P. Forn-Díaz, R. Belyansky, J. L. Orgiazzi, M. A. Yurtalan, M. R. Otto, A. Lupascu, C. M. Wilson, and M. Grifoni, *Nat. Commun.* **9**, 1403 (2018).
- [20] L. E. Bruhat, J. J. Viennot, M. C. Dartiailh, M. M. Desjardins, A. Cottet, and T. Kontos, *Phys. Rev. B* **98**, 075121 (2018).
- [21] A. Kaminski, Y. V. Nazarov, and L. I. Glazman, *Phys. Rev. B* **62**, 8154 (2000).
- [22] A. Kogan, S. Amasha, and M. A. Kastner, *Science* **304**, 1293 (2004).
- [23] K. Le Hur, *Phys. Rev. B* **85**, 140506(R) (2012).
- [24] K. Le Hur, L. Henriët, A. Petrescu, K. Plekhanov, G. Roux, and M. Schiró, *C. R. Phys.* **17**, 808 (2016).
- [25] L. Borda, G. Zarand, W. Hofstetter, B. I. Halperin, and J. von Delft, *Phys. Rev. Lett.* **90**, 026602 (2003).
- [26] M.-R. Li and K. Le Hur, *Phys. Rev. Lett.* **93**, 176802 (2004).
- [27] C. Mora, P. Vitushinsky, X. Leyronas, A. A. Clerk, and K. Le Hur, *Phys. Rev. B* **80**, 155322 (2009).
- [28] K. Le Hur, P. Simon, and D. Loss, *Phys. Rev. B* **75**, 035332 (2007).
- [29] P. Nozières, *J. Low Temp. Phys.* **17**, 31 (1974).
- [30] H. Shiba, *Prog. Theor. Phys.* **54**, 967 (1975).
- [31] M. Garst, P. Wölfle, L. Borda, J. von Delft, and L. Glazman, *Phys. Rev. B* **72**, 205125 (2005).
- [32] C. Mora and K. Le Hur, *Nat. Phys.* **6**, 697 (2010).
- [33] M. Filippone, K. Le Hur, and C. Mora, *Phys. Rev. Lett.* **107**, 176601 (2011).
- [34] J. Gabelli, G. Fève, J. M. Berroir, Plaçais, A. Cavanna, B. Etienne, Y. Jin, and D. C. Glattli, *Science* **313**, 499 (2006).
- [35] M. Filippone, A. Marguerite, K. Le Hur, G. Fève, and C. Mora, *Entropy* **22**, 847 (2020).
- [36] M. Büttiker, A. Prêtre, and H. Thomas, *Phys. Rev. Lett.* **70**, 4114 (1993).
- [37] M. Schiró and K. Le Hur, *Phys. Rev. B* **89**, 195127 (2014).
- [38] A. A. Clerk, M. H. Devoret, S. M. Girvin, F. Marquardt, and R. J. Schoelkopf, *Rev. Mod. Phys.* **82**, 1155 (2010).
- [39] T. Delattre, C. Feuillet-Palma, L. Herrmann, P. Morfin, J.-M. Berroir, G. Fève, B. Plaçais, D. Glattli, M.-S. Choi, C. Mora, and T. Kontos, *Nat. Phys.* **5**, 208 (2009).
- [40] M. Delbecq, L. Bruhat, J. Viennot, S. Datta, A. Cottet, and T. Kontos, *Nat. Commun.* **4**, 1400 (2013).
- [41] J.-H. Chen, L. Li, W. G. Cullen, D. Williams, and M. S. Fuhrer, *Nat. Phys.* **7**, 535 (2011).
- [42] M. Eich, F. Herman, R. Pisoni, H. Overweg, A. Kurzmam, Y. Lee, P. Rickhaus, K. Watanabe, T. Taniguchi, M. Sigríst, T. Ihn, and K. Ensslin, *Phys. Rev. X* **8**, 031023 (2018).
- [43] M. Raith, C. Ertler, P. Stano, M. Wimmer, and J. Fabian, *Phys. Rev. B* **89**, 085414 (2014).
- [44] A. Kurzmam, Y. Kleeorin, T. Chuyao, R. Garreis, A. Knothe, M. Eich, C. Mittag, C. Gold, F. K. de Vries, K. Watanabe, T. Taniguchi, V. Fal'ko, Y. Meir, T. Ihn, and K. Ensslin, *arXiv:2103.04864*.
- [45] J. Hopkinson, K. Le Hur, and E. Dupont, *Eur. Phys. J. B* **48**, 429 (2005).
- [46] L.-J. Wang, G.-P. Guo, D. Wei, G. Cao, T. Tu, M. Xiao, G.-C. Guo, and A. M. Chang, *Appl. Phys. Lett.* **99**, 112117 (2011).
- [47] L. J. Wang, H. O. Li, T. Tu, G. Cao, C. Zhou, X. J. Hao, Z. Su, M. Xiao, G. C. Guo, A.-M. Chang, and G.-P. Guo, *Appl. Phys. Lett.* **100**, 022106 (2012).
- [48] G.-W. Deng, D. Wei, S.-X. Li, J. R. Johansson, W.-C. Kong, H.-O. Li, G. Cao, M. Xiao, G.-C. Guo, F. Nori *et al.*, *Nano Lett.* **15**, 6620 (2015).
- [49] G.-W. Deng, D. Wei, J. R. Johansson, M.-L. Zhang, S.-X. Li, H.-O. Li, G. Cao, M. Xiao, T. Tu, G.-C. Guo, H.-W. Jiang, F. Nori, and G.-P. Guo, *Phys. Rev. Lett.* **115**, 126804 (2015).
- [50] I. Affleck and A. W. W. Ludwig, *Phys. Rev. B* **48**, 7297 (1993).
- [51] H. Max, D. Frank, K. Andreas, G. Jan, B. Alexander, E. Peter, F. Kirill, F. Michael, P. M. Edwin, J. S. Manuel *et al.*, *arXiv:1506.09114*.
- [52] K. Le Hur, L. Henriët, L. Herviou, K. Plekhanov, A. Petrescu, T. Goren, M. Schiro, C. Mora, and P. P. Orth, *C. R. Phys.* **19**, 451 (2018).
- [53] C. W. Gardiner and M. J. Collett, *Phys. Rev. A* **31**, 3761 (1985).
- [54] A. Rosch, J. Kroha, and P. Wölfle, *Phys. Rev. Lett.* **87**, 156802 (2001).
- [55] Z. Iftikhar, S. Jezouin, A. Anthore, U. Gennser, F. D. Parmentier, A. Cavanna, and F. Pierre, *Nature (London)* **526**, 233 (2015).
- [56] S. J. Chorley, M. R. Galpin, F. W. Jayatilaka, C. G. Smith, D. E. Logan, and M. R. Buitelaar, *Phys. Rev. Lett.* **109**, 156804 (2012).
- [57] J. Hutchinson and K. Le Hur, *Commun. Phys.* **4**, 144 (2021).
- [58] D. Wei, H.-O. Li, G. Cao, G. Luo, Z.-X. Zheng, T. Tu, M. Xiao, G.-C. Guo, H.-W. Jiang, and G.-P. Guo, *Sci. Rep.* **3**, 3175 (2013).
- [59] G.-L. Ingold and Y. V. Nazarov, *arXiv:Cond-Mat/0508728*.
- [60] R. Ziegler, C. Bruder, and H. Schoeller, *Phys. Rev. B* **62**, 1961 (2000).
- [61] A. H. Castro Neto, F. Guinea, N. M. R. Peres, K. S. Novoselov, and A. K. Geim, *Rev. Mod. Phys.* **81**, 109 (2009).
- [62] R. Egger and O. Gogolin, *Eur. Phys. J. B* **3**, 281 (1998).
- [63] K. Le Hur, S. Vishveshwara, and C. Bena, *Phys. Rev. B* **77**, 041406(R) (2008).
- [64] L. Childress, A. S. Sorensen, and M. D. Lukin, *Phys. Rev. A* **69**, 042302 (2004).
- [65] K. D. Petersson, L. W. McFaul, M. D. Schroer, M. Jung, J. M. Taylor, A. H. Houck, and J. R. Petta, *Nature (London)* **490**, 380 (2012).
- [66] A. Cottet, T. Kontos, and B. Douçot, *Phys. Rev. B* **88**, 195415 (2013).
- [67] K. Le Hur, P. Simon, and L. Borda, *Phys. Rev. B* **69**, 045326 (2004).
- [68] R. Lopez, D. Sanchez, M. Lee, M.-S. Choi, P. Simon, and K. Le Hur, *Phys. Rev. B* **71**, 115312 (2005).
- [69] S. Sasaki, S. Amaha, N. Asakawa, M. Eto, and S. Tarucha, *Phys. Rev. Lett.* **93**, 017205 (2004).